NITROGEN-COORDINATED METAL ELECTROCATALYSTS FOR OXYGEN REDUCTION REACTION

by
Pingfan Hu

A thesis submitted to Johns Hopkins University in conformity with the requirements for the degree of Master of Science in Engineering

Baltimore, Maryland

May 2019

Abstract

Proton Exchange Membrane Fuel Cells (PEMFC) have attracted substantial attention for power delivery due to their relatively low working temperature, fast start-up, large current density and high efficiency. They can be applied for a range of devices from automotive applications to portable digital equipments.

Unfortunately, the cost of the catalytic materials needed to build a PEMFC is quite high. Replacing precious metal electrocatalysts with high-performance and low-cost nonprecious metal electrocatalysts is crucial for the commercialization of fuel cell technologies.

The work performed within this thesis reports a novel and facile method to successfully synthesize iron-, cobalt-, and nitrogen-codoped nanocarbon (NC)-based electrocatalysts (Fe, Co, N-NC) by one-step pyrolysis of an iron-, cobalt-bimetal zeolitic imidazolate framework (Fe, Co-ZIF) nanocrystal precursors. The optimized Fe, Co, N-NC (2.7:1) (Fe/Co molar ratio of 2.7:1 in Fe, Co-ZIF) electrocatalyst exhibited a highly promising activity for oxygen reduction reaction with a positive half-wave potential ($E_{1/2}$) of 0.731 V. The active sites of the electrocatalysts were analyzed through the nitrogen monoxide temperature programmed desorption.

Committee: Dr. Chao Wang (Advisor)

Dr. Michael Tsapatsis

Acknowledgements

I would like to express my sincere gratitude to my advisor Dr. Chao Wang, for giving me the chance to join the Wang Lab. The research experience not only enhances my knowledge and understanding of different research methodologies but provides me with insightful advice about my future academic plans as well. It's a pleasure and honor to be a part of the group. Also, I would like to thank Dr. Michael Tsapatsis to be my committee member.

I would like to express my deepest appreciation to Dr. Yifan Liu, whom I worked with during these two years. Yifan is a great mentor and friend. It would be impossible to count all the ways that he has helped me in my life. His guidance helped me in all the time of research and writing of this thesis.

The other members of the Wang Lab have also provided me with great help. I would like to especially thank Zhongyu Liu and Wenqi Zhou for the time we were working together. I would like to thank my old friends Ying yin from Ohio State University and Kairui Zhang from University of Wisconsin-Madison for their help in my life. Also, I thank my friends Yutian Qian from Dr. Donohue lab and Nianchao Wang from Dr. Konstantopoulos lab for all the fun we have had in the last two years.

Last but not the least, I would like to thank my parents for their love and support. I would like to thank my girlfriend, Yingjia, for showing up in my life. I love you to the Icarus and back.

Table of Contents

1 Introduction 1

1.1. Motivation 1

1.2. Proton Exchange Membrane Fuel Cells (PEMFC) 2

1.3. Transition metal and nitrogen-doped carbon (M-N-C) 4

1.4. Zeolitic imidazolate frameworks-8 (ZIF-8) 6

1.5. Temperature programmed desperation (TPD) 8

2 Experimental Methods 10

2.1. Synthesis 10

2.1.1. Single metal/Bimetal-ZIF nanocrystals synthesis 11

2.1.2. Pyrolysis for nitrogen-doped carbon with metal nanoparticles.....14

2.1.3. Synthetic route for whole process 16

2.2. Material characterization 17

2.2.1. Transmission Electron Microscopy (TEM) 18

2.2.2. Inductively Coupled Plasma Mass Spectrometry (ICP-MS) 19

2.2.3. X-ray Powder Diffraction (XRD) 23

2.3. Electrochemical Measurements 25

2.4. Temperature programmed desperation measurements.....27

2.4.1. Prepare the samples…….....27

2.4.2. Main TPD process …….....28

2.4.3. After the experiment...…….....30

3 Discussion and results 31

3.1. Synthesis method …….....31

3.2. Electrochemical results analysis 32

3.3. Temperature programmed desperation results analysis 39

4 Conclusions 40

5 References 41

List of Tables:

Table 2-1 Experiment reagents for the single metal zeolitic imidazolate framework 11

Table 2-2 Experiment reagents for the bimetal zeolitic imidazolate framework 13

Table 2-3 ICP test result of single metal in the single metal-ZIF 19

Table 2-4 ICP test result of bimetal in the double metal-ZIF..... 19

Table 3-1 Cathodic peaks of single metal and nitrogen-doped NC-based electrocatalysts in O_2-saturated (V) 33

List of Figures:

Figure 1-1 Phenomena in PEMFC: two-dimensional sectional view[1] 2

Figure 1-2 The single crystal x-ray structure of ZIF-8 sod. (Left and Center) The net is shown as a stick diagram (Left) and as a tiling (Center). The largest cage in each ZIF is shown with ZnN4 tetrahedra in blue (Right)[17]..... 7

Figure 1-3 Sodalite topology (Left) and narrow six-membered-ring opening through which molecules have to pass (Right)[21]..... 8

Figure 1-4 Experimental setup of the temperature programmed desorption system 9

Figure 2-1 Change of the solution during the synthesis of Co-ZIF nanocrystals 12

Figure 2-2 Tube furnace for pyrolysis 14

Figure 2-3 Single metal ZIF before and after pyrolysis 15

Figure 2-4 Bimetal ZIF before and after pyrolysis 15

Figure 2-5 Schematic illustration of the synthetic route for nitrogen-doped carbon with single metal nanoparticles 16

Figure 2-6 Schematic illustration of the synthetic route for nitrogen-doped carbon with bimetal nanoparticles 16

Figure 2-7 TEM images of single metal nanocrystals before and after pyrolysis 18

Figure 2-8 TEM images of bimetal nanocrystals before and after pyrolysis 18

Figure 2-9 Calibration curves of Co concentration used in ICP test.....20

Figure 2-10 Calibration curves of Fe concentration used in ICP test.....20

Figure 2-11 Calibration curves of Mn concentration used in ICP test.....20

Figure 2-12 Calibration curves of Ni concentration used in ICP test.....21

Figure 2-13 Calibration curves of Cu concentration used in ICP test.....21

Figure 2-14 XRD of Bimetal-ZIF nanocrystals before pyrolysis 23

Figure 2-15 XRD of Bimetal-ZIF nanocrystals after pyrolysis 23

Figure 2-16 Set up for the electrochemical measurements 26

Figure 2-17 The glassy carbon electrode (working electrode) with catalyst 26

Figure 2-18 Sample tube assembly of temperature programmed desorption system 28

Figure 2-19 Command window of temperature programmed desorption 29

Figure 3-1 Cyclic voltammetry curves of Co/ Fe/ Ni/ Cu/ Mn-NC recorded in Argon- and O_2-saturated 0.1m H_2SO_4 32

Figure 3-2 Linear sweep voltammetry curves for different materials in O_2- saturated 0.5M H_2SO_4 with rotation rate of 1600 rpm. 34

Figure 3-3 Linear sweep voltammetry curves of five single metal NC measured at different rotation rates 35

Figure 3-4 Linear sweep voltammetry curves of five single metal NC measured at different rotation rates and the volcano plot of electron transfer numbers for all samples 35

Figure 3-5 Cyclic voltammetry curves of Co/ Fe/ CoFe -NC recorded in Argon- and carbon monoxide -saturated 0.5M H_2SO_4 36

Figure 3-6 Linear sweep voltammetry curves for different materials in O_2- saturated 0.5M H_2SO_4 with rotation rate of 1600 rpm. 37

Figure 3-7 Volcano plot for the absolute current density at 0.7 (half wave potential) 37

Figure 3-8 Linear sweep voltammetry curves of three bimetal NC measured at different rotation rates 38

Figure 3-9 Electron transfer numbers for all samples 38

Figure 3-10 Temperature programmed desorption analysis for bimetal NC 39

1 Introduction

1.1. Motivation

The purpose behind the work presented in this thesis is to reduce the cost of the proton exchange membrane fuel cells (PEMFC) by enhancing the catalytic activity of zeolitic imidazolate frameworks-8-derived nitrogen-doped carbon with incorporated metal nanoparticles in the oxygen reduction reaction (ORR). We combined the study of nano-material synthesis, electro-chemical catalytic reactions and temperature programmed desorption (TPD) to optimize the electrocatalysts and analyze their active sites.

This thesis presents the synthesis of five single transition metal nitrogen-doped nanocarbon (NC)-based electrocatalysts (Mn/ Fe/ Co/ Ni/ Cu, N-NC) and a bimetal nitrogen-codoped nanocarbon (NC)-based electrocatalyst (Fe, Co, N-NC) with iron-, cobalt-bimetal zeolitic imidazolate framework (Fe, Co-ZIF) nanocrystal precursors at three Fe/Co molar ratios (1:1, 2.7:1, 6.4:1). The electrocatalysts were characterized by Transmission Electron Microscopy (TEM), Inductively Coupled Plasma Mass Spectrometry (ICP-MS) and X-ray Diffraction (XRD). After that, the ORR catalytic activities were investigated by cyclic voltammetry (CV) curves, linear sweep voltammetry (LSV) curves and Koutecký–Levich analysis (K-L analysis). Finally, the active sites of the electrocatalysts were analyzed by TPD measurements.

The remainder of this introduction is introducing the theory and techniques behind the application, nano-material synthesis, electro-chemical catalytic reactions and TPD.

1.2. Proton Exchange Membrane Fuel Cells

The PEMFC is a two-electrode system that convert the chemical energy stored in hydrogen fuel directly and efficiently to electrical energy with water as the only byproduct.

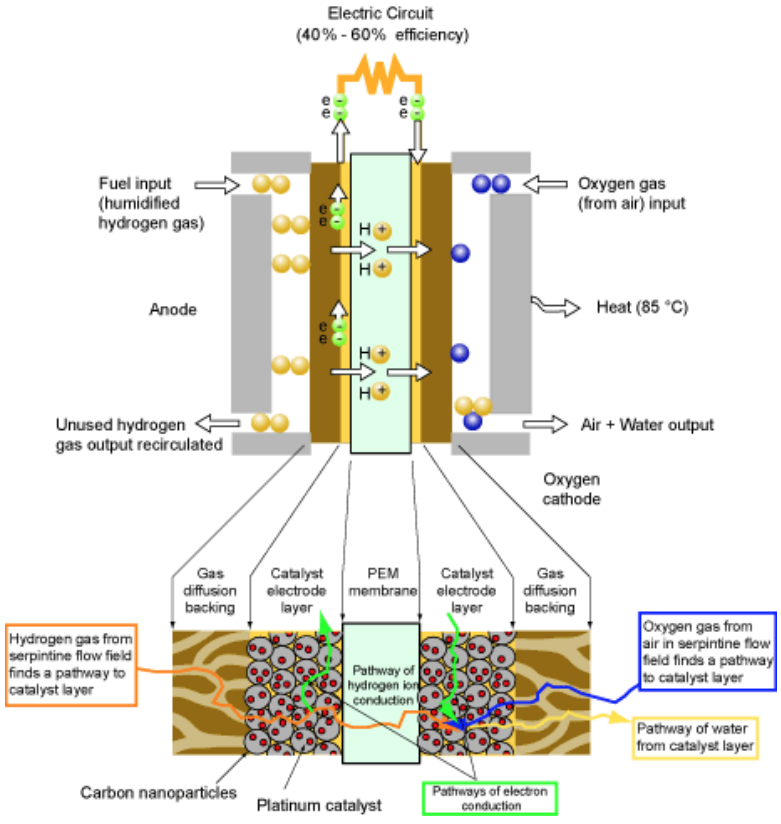

Figure 1-1 Phenomena in a PEMFC: two-dimensional sectional view[1]

Fig. 1-1 shows the phenomena in a PEMFC. Humidified hydrogen gas and oxygen gas from air are forced to flow down the anode and cathode gas flow channels, respectively. Hydrogen

gas and oxygen gas flow through the respective gas diffusion layers and diffuse into the respective catalyst layers. On the anode catalyst layer of the PEMFC, hydrogen oxidation reaction (HOR) occurs, forming protons and electrons, equation 1.

$$H_2 \rightarrow 2H^+ + 2e^- \qquad E^0_a = 0\ V \tag{1}$$

The generated electrons are conducted via carbon support to the anode current collector, and then to the cathode current collector via an external circuit while the generated protons transport through the membrane. Oxygen reduction reaction (ORR) occurs when oxygen is reduced with protons and electrons at the cathode catalyst layer to form water, equation 2.

$$O_2 + 4H^+ + 4e^- \rightarrow 2H_2O \qquad E^0_c = 1.23\ V \tag{2}$$

Product water is transported out of the cathode catalyst layer, through cathode gas diffusion layer, and eventually out of the cathode gas flow channels. As the electrons pass through the external circuit, energy from the electrons is utilized[2].

Combining equations 1 and 2 shows the full reaction in the PEMFC, equation 3

$$2H_2 + O_2 \rightarrow 2H_2O \tag{3}$$

Within this system, the catalyst widely used for both the anode and the cathode is platinum nanoparticle catalysts, supported on high surface area carbonaceous materials. However, the expensive price and rarity of platinum have limited its widespread implementation in PEMFCs, especially for the ORR at the cathode that accounts for approximately 80% of the platinum loading in fuel cell electrodes[3]. At the current market price, the platinum needed for powering up a mid-

range fuel cell vehicle may cost more than $1,800 (about 60 mg platinum). The amount needed for a diesel autocatalyst, in comparison, is worth just over $200[4]. Therefore, platinum-loading reduction is important for commercialization of PEMFCs. While lowering the Pt-loading for hydrogen-fed anode electrodes from today's 0.2–0.4 down to 0.05 mg Pt/cm^2 is straightforward due to the large activity of Pt toward the HOR, a lowering of oxygen-fed cathode loadings of about 0.4 mg Pt/cm^2 is limited by the poor activity of Pt for the ORR[5]. To overcome this bottleneck, one approach is to find a nonprecious platinum group metal (PGM)-free catalyst for the cathode.

1.3. Transition metal and nitrogen-doped carbon

The PGM-free catalysts for the ORR have been studied extensively due to their potential to dramatically lower the cost of PEMFCs. Among studied formulations, the transition metal and nitrogen-doped carbon nanomaterials (M-N-C) have attracted great attention because of their excellent electrocatalytic performance, promising stability, and low-cost scalable synthesis[3,6-8].

Chemical doping is a potential method for carbon materials to increase free charge-carrier densities and enhance the electrical or thermal conductivities[9]. Compare with other potential dopants of carbon materials, nitrogen is considered to be an excellent choice because of the comparable atomic sizes of both nitrogen and carbon elements and the five valence electrons nitrogen contains for forming strong valence bonds with carbon atoms. There are two types of doping nitrogen. Pyridinic nitrogen is obtained by doping at the edge of the graphene layer and

quaternary nitrogen is obtained by doping at in-plane[10]. For the ORR, nitrogen could improve the ability of carbon to reduce oxygen since the nitrogen atom could stabilize the metal atom and prevent the metal atom from oxidation and dissolution in acid. It was experimentally found that nitrogen atoms, viewed as an n-type dopant, can be readily incorporated into the carbon lattice. When it replaces carbon in the graphite matrix, the carbon plane will contain an extra electron that is more easily donated to oxygen[11]. Also, compare with undoped carbon black, nitrogen-doped carbons have higher surface polarity so that it exhibits a faster charge-transfer rate at the electrode/ electrolyte interface and favorable to the proton and electron transfer in the ORR[12].

Adding transition metal to the nitrogen-doped carbon for the ORR has been investigated since the codoping of the transition metals would further enhance the performance of the catalysts. Although the importance of the codoping of transition metals has been verified, the role and the mechanism of the doped transition metals in the catalyst, as well as the effects of various transition metals, still remains unclear[13]. It was reported that the ORR activity of the catalysts follows the order of Fe > Co > Zn > Mn > Cu > Ni in both acid and alkaline electrolytes[14].

Another important factor for the nitrogen doping is heat-treatment temperature. By tuning the temperature of heat-treatment, the content and relative ratios of different types of doped nitrogen can be controlled in both Fe- and Co-based catalysts. The increase of the temperature from 800 to 1000 °C leads a decrease in the total nitrogen content and an increase in the ratio of quaternary-to-pyridinic nitrogen. However, the ORR activity does not necessarily change under

the temperature raise[15]. It indicates that quaternary nitrogen and the optimal C-N_x structures are likely a crucial part of the ORR active site(s). Also, the heat-treatment temperature governs the catalyst morphology which strongly influence the ORR activity. Heat treatment at even higher temperatures like 1500 °C are conducted and the catalysts yields less uniform morphology and containing particles significantly larger than lower temperature with ORR activity gradually lost[3].

1.4. Zeolitic imidazolate frameworks-8 (ZIF-8)

People used to synthesize M–N–C catalysts through the pyrolysis of carbon and nitrogen precursors, metal salts, and carbon supports[16]. However, the aggregation of unstable metallic compounds attached in graphitic carbon shells is caused by the uncontrolled heat treatment. To remove these inactive metal species that reduce catalyst activity and stability for ORR, additional acid-leaching treatment is required. A second heat treatment is needed to repair the damaged carbon structures after the acid leaching process[17]. Currently, most M–N–C catalysts exhibit much better ORR catalytic performance in alkaline electrolytes than in acidic electrolytes. The bad performance in acidic media cause by the inactive metal aggregates, such as metallic particles, carbides, nitrides, and oxides[18].

To overcome these problems, zeolitic imidazolate frameworks (ZIFs) have emerged as a new platform for the synthesis of M-N-C catalysts. ZIFs, as a subclass of metal−organic framework (MOF) materials, have been treated as the promising precursors to synthesize M−N−C

electrocatalysts for ORR because of their large specific surface area and ordered M−N_4 coordination substructures. In the skeleton of the ZIF, metal atoms bridge with ligands to form 3D crystal frameworks with high porosity, surface area, high thermal and chemical stability. These ZIF precursors can be converted to porous nitrogen-doped carbon through heat treatment. Moreover, the original metal-nitrogen bond connected with hydrocarbon networks could directly yield M-N_x sites that are active for the ORR in acid[19].

Among different ZIFs like ZIF-2 crb, ZIF-3 dft, ZIF-4 cag, ZIF- 5 gar, ZIF-6 gis, ZIF-8 sod, ZIF-10 mer, ZIF-11 rho, ZIF-8 sod is the most suitable one for the M-N-C catalyst because of its suitable ring size and best chemical stability. The single crystal x-ray structure of ZIF-8 sod is shown in Figure 1-2[20] and the ring structure of ZIF-8 sod is shown in Figure 1-3. The size of the six-membered ring pores is ~3.4 Angstrom[21].

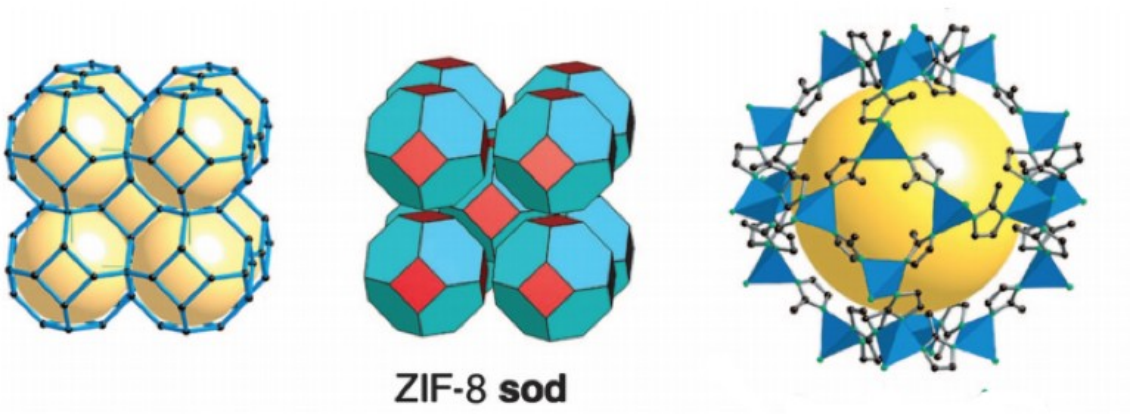

Figure 1-2 The single crystal x-ray structure of ZIF-8 sod. (Left and Center) The net is shown as a stick diagram (Left) and as a tiling (Center). The largest cage in ZIF-8 is shown with ZnN4 tetrahedra in blue (Right)

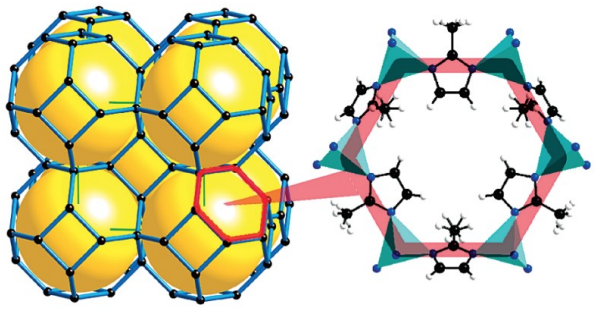

Figure 1-3 Sodalite topology (Left) and six-membered-ring opening through which molecules have to pass (Right)

1.5. Temperature programmed desorption

The number, type, and strength of active sites on the surface of a catalyst can be determined by TPD through measurement of the amount of gas desorbed at different temperatures. A steady stream of analysis gas flows through the sample and adsorbs on the active sites after the sample was prepared. TPD begins raising the temperature linearly with time while a steady stream of inert carrier gas flows through the sample to get rid of the excess adsorbed gas on the surface. At a certain temperature, the bond between the adsorbate and adsorbent will break and the adsorbed species desorb since the heat overcomes the activation energy. If different active metals are present, since chemical bonds between each metal and the adsorbed molecule have different energy, the desorbed temperature for different active metals are also different. These desorbed molecules enter the stream of inert carrier gas and are swept by the thermal conductivity detector (TCD). TCD measures the gas concentrations. The number and strength of active sites can be determined by the volume of desorbed species, the stoichiometry factor and the desorbed temperature[22].

Figure 1-4 Experimental setup of TPD system

The figure 1-4 shows the experimental setup of our TPD system. The system consists of an AutoChem 2920 Automated Catalyst Characterization System and a GSD 320 Gas Analysis System. The samples are prepared at the AutoChem 2920 Automated Catalyst Characterization System and the desorbed gas are analyzed by the GSD 320 Gas Analysis System. The detailed procedures will be discussed in the experimental methods system.

2 Experimental Methods

2.1. Synthesis

Chemicals. Zinc (II) nitrate ($Zn(NO_3)_2$), Cobalt (II) nitrate ($Co(NO_3)_2$), Iron (III) acetylacetonate ($Fe(acac)_3$), Nickel (II) acetylacetonate ($Ni(acac)_2$), Copper (II) acetylacetonate ($Cu(acac)_2$), Manganese (II) acetylacetonate ($Mn(acac)_2$) and methanol were purchased from Sigma Aldrich. The protocol for the synthesis will be further discussed in the discussion and results section.

2.1.1 Single metal/Bimetal-ZIF nanocrystals synthesis

Table 2-1 Experiment reagents for the single metal zeolitic imidazolate framework

	element	salt	molar	Molar mass	weight
Metal salt	Co	$Co(NO_3)_2$	2.5mmol	291.03g/mol	0.7276g
	Fe	$Fe(acac)_3$	2.5mmol	353.17g/mol	0.8779g
	Ni	$Ni(acac)_2$	2.5mmol	256.91g/mol	0.6423g
	Cu	$Cu(acac)_2$	2.5mmol	261.76g/mol	0.6544g
	Mn	$Mn(acac)_2$	2.5mmol	253.15g/mol	0.6329g

	element	salt	molar	Molar mass	weight
Metal salt	Zn	$Zn(NO_3)_2$	10mmol	297.49g/mol	2.9749g

		molar	Molar mass	weight
Precursor	2-methylimidazole	0.1mol	82.1g/mol	8.21g

For the single metal zeolitic imidazolate framework nanocrystals synthesis, each metal salt ($Co(NO_3)_2$, $Fe(acac)_3$, $Ni(acac)_2$, $Cu(acac)_2$, $Mn(acac)_2$) was dissolved with 10 mmol $Zn(NO_3)_2$ in the methanol (250 ml) containing 2.5 mmol metal salt ($Co(NO_3)_2$, $Fe(acac)_3$, $Ni(acac)_2$, $Cu(acac)_2$, $Mn(acac)_2$). The solution was covered with parafilm and sonicated. Then, the abovementioned solution was poured into another methanol solution (250 ml) containing 2-methylimidazole (8.21 g). After 24 hours, the solution became transparent and precipitate formed at the bottom of flask. Figure 2-1 showed the change of the solution during the synthesis of Co-ZIF nanocrystals. The color change is caused by the Zn(II) cations be substituted by Co(II) and forms $Co_xZn_{1-x}(HmIm)_2$ coordination complex without altering its topology[23].

solution1 (2-methylimidazole)

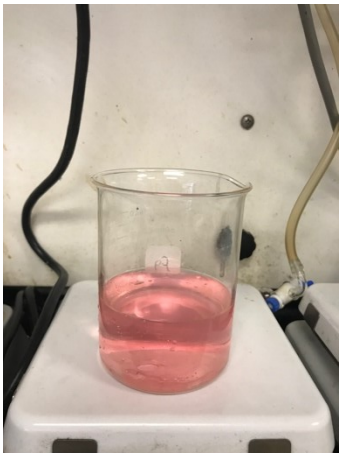

solution2 ($Zn(NO_3)_2$ + $Co(NO_3)_2$)

right after mixing
solution 1 and solution 2

after mixing for 24 hours

Figure 2-1 Change of the solution during the synthesis of Co-ZIF nanocrystals

The solution was collected by 50 ml centrifuge tubes and the centrifuge tubes were centrifuged at 10000 RPM for 5 minutes to precipitate out the metal-ZIF nanocrystals from the solution. After that, the metal-ZIF nanocrystals were then re-dispersed and sonicated in 40 ml methanol and centrifuged at 10000 RPM for 20 minutes to precipitate out the metal-ZIF nanocrystals. Repeated this procedure two times. The metal-ZIF nanocrystals were dried in a Quincy Lab Model 20 lab oven set at 80C overnight. At the end, the nanocrystals were weighed and collected for pyrolysis.

Table 2-2 Experiment reagents for the bimetal zeolitic imidazolate framework

	Ratio		molar		weight	
	Fe	Co	Fe	Co	Fe	Co
Metal salt	4	1	2.0mmol	0.5mmol	0.7063g	0.1451g
	16	1	2.35mmol	0.15mmol	0.8310g	0.0428g
	64	1	2.462mmol	0.0384mmol	0.8693g	0.0112g

	element	salt	molar	Molar mass	weight
Metal salt	Zn	$Zn(NO_3)_2$	10mmol	297.49g/mol	2.9749g

		molar	Molar mass	weight
Precursor	2-methylimidazole	0.1mol	82.1g/mol	8.21g

For the bimetal metal zeolitic imidazolate framework nanocrystals synthesis. It was quite similar to the single metal zeolitic imidazolate framework nanocrystals synthesis. The main difference was that the total molar amount of two metal salts ($Fe(acac)_3$ and $Co(NO_3)_2$) were kept the same (2.5 mmol) while the ratios of Fe/Co were varied from 4:1, 16:1 and 64:1. The actual ratios of the Fe/Co were determined by Inductively Coupled Plasma Mass Spectrometry (ICP-MS). The ratios were 1:1, 2.7:1 and 6.4:1.

2.1.2 Pyrolysis for nitrogen-doped carbon with metal nanoparticles

After the metal-ZIF nanocrystals were weighed and collected, nitrogen-doped carbon with metal nanoparticles were synthesized by pyrolysis at 1100 °C in a tube furnace under nitrogen for 1 h. The pyrolysis process was shown in Figure 2-2, the tube was saturated with nitrogen for 30 minutes, then the temperature start raising with the ramping rate at 10C/min. After the temperature reached 1100C, the temperature was kept at 1100C for 1 hr. The nitrogen-doped carbon with metal nanoparticles were collected after the temperature dropped automatically. The whole process except for cooling took about 4.5 hrs. The single metal/bimetal ZIF samples before and after pyrolysis were shown in Figure 2-3 and Figure 2-4. The color of the powder changed to black because majority of the sample was carbon after pyrolysis at 1100 °C.

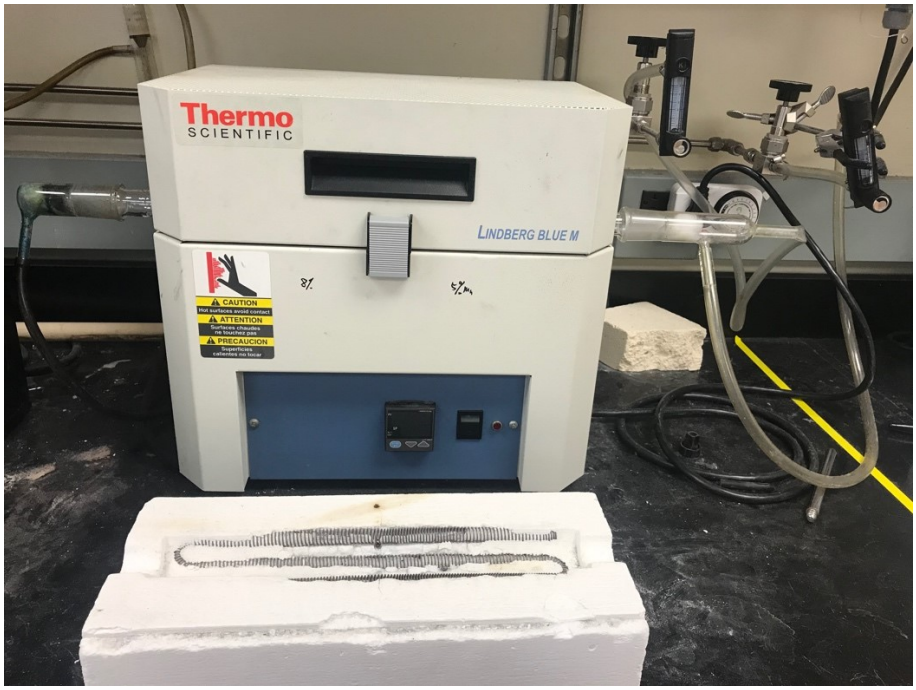

Figure 2-2 Tube furnace for pyrolysis

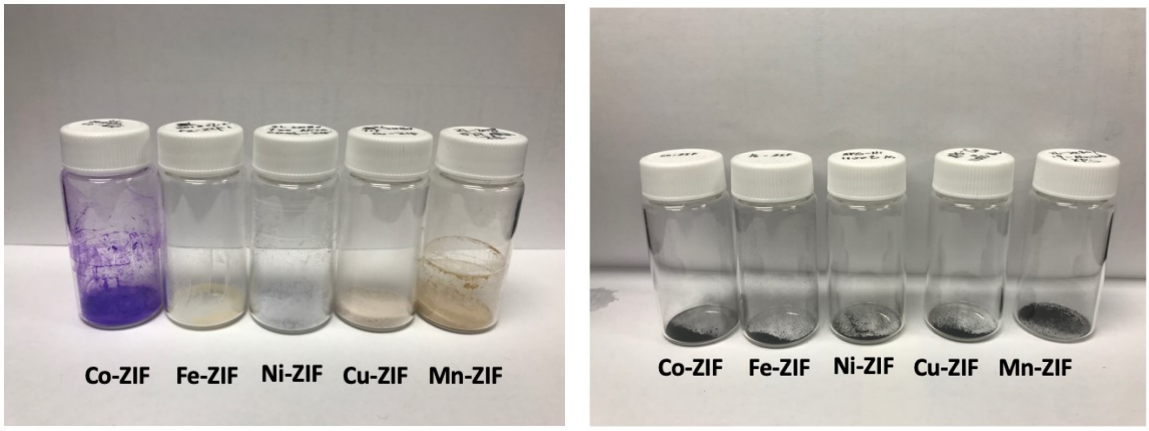

Figure 2-3 Single metal-ZIF nanocrystals before and after pyrolysis

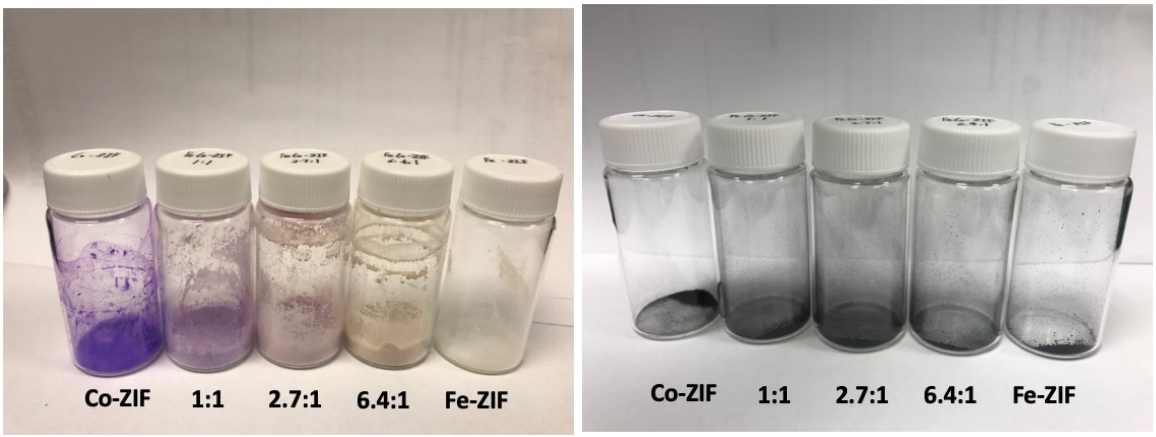

Figure 2-4 Bimetal-ZIF nanocrystals before and after pyrolysis

2.1.3 The synthetic route for whole process

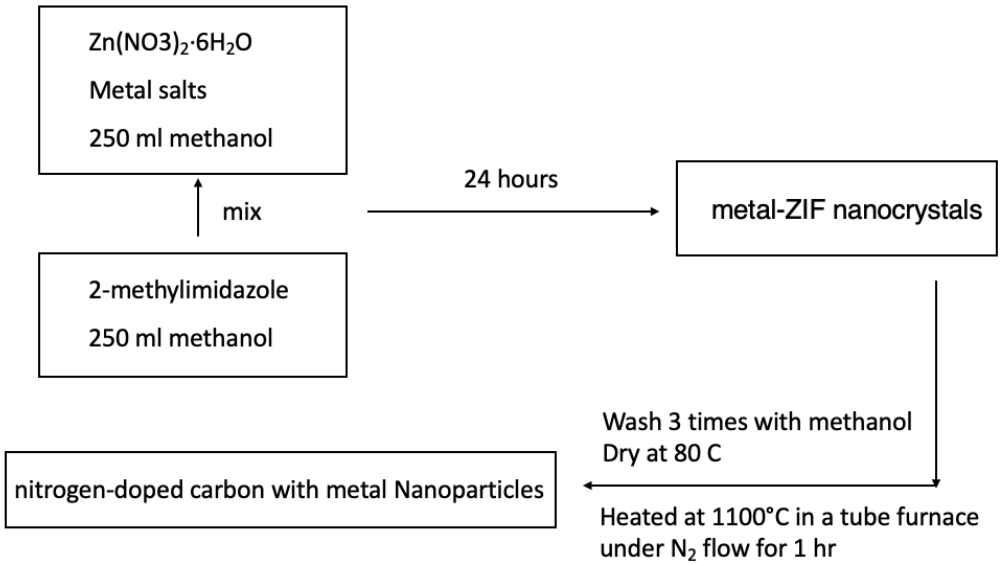

Figure 2-5 Schematic illustration of the synthetic route for nitrogen-doped carbon with single metal nanoparticles

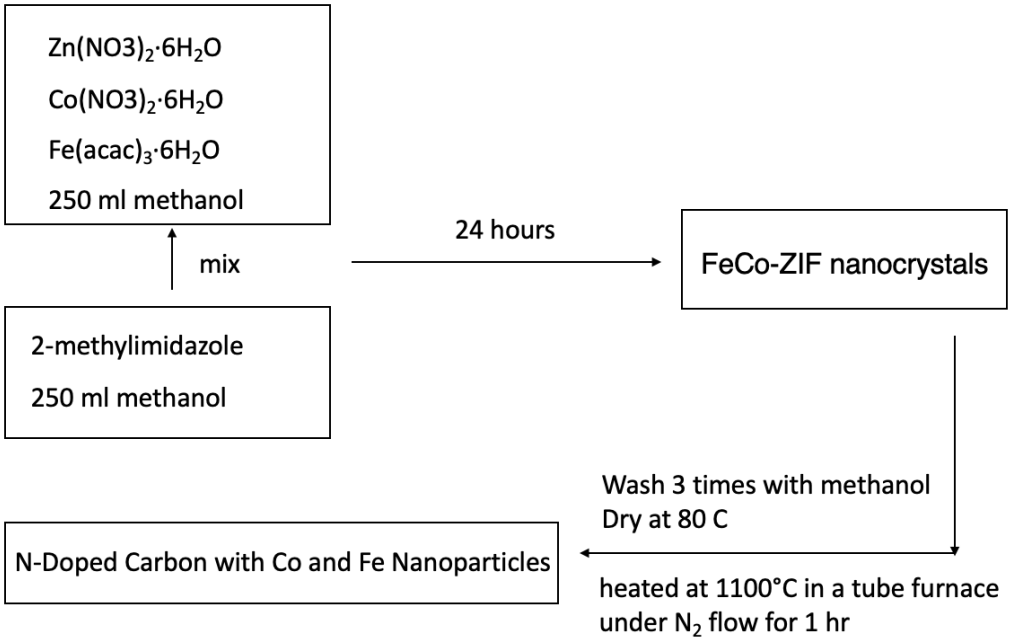

Figure 2-6 Schematic illustration of the synthetic route for nitrogen-doped carbon with bimetal nanoparticles

2.2 Material characterization

Transmission Electron Microscopy (TEM) images were acquired on a FEI Tecnai 12 microscope operated at 100 kV. Inductively Coupled Plasma Mass Spectrometry (ICP-MS) was collected with a PerkinElmer Elan DRC II Quadrupole. X-ray diffraction (XRD) patterns were collected on a PANalytical X'Pert^3 Powder X-Ray Diffractometer equipped with a Cu Kα radiation source (λ=0.15406).

2.2.1. Transmission Electron Microscopy (TEM)

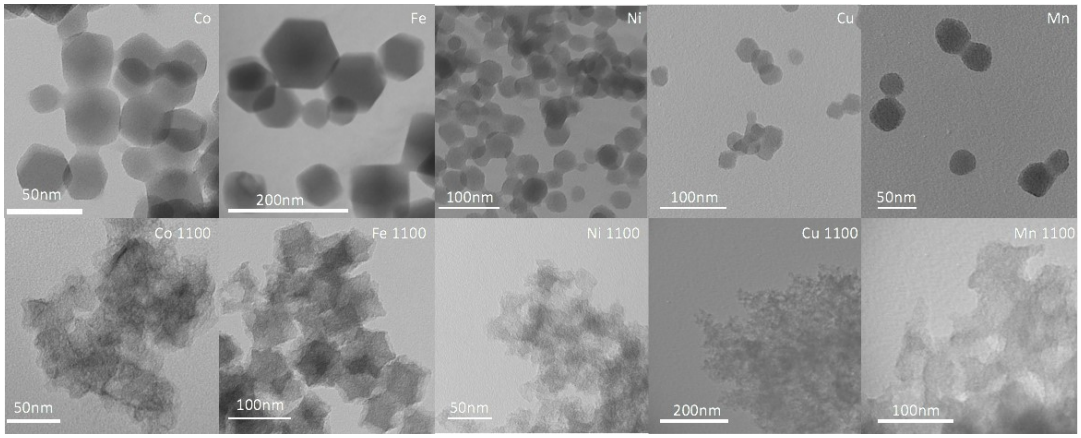

Figure 2-7 TEM images of single metal-ZIF nanocrystals before and after pyrolysis

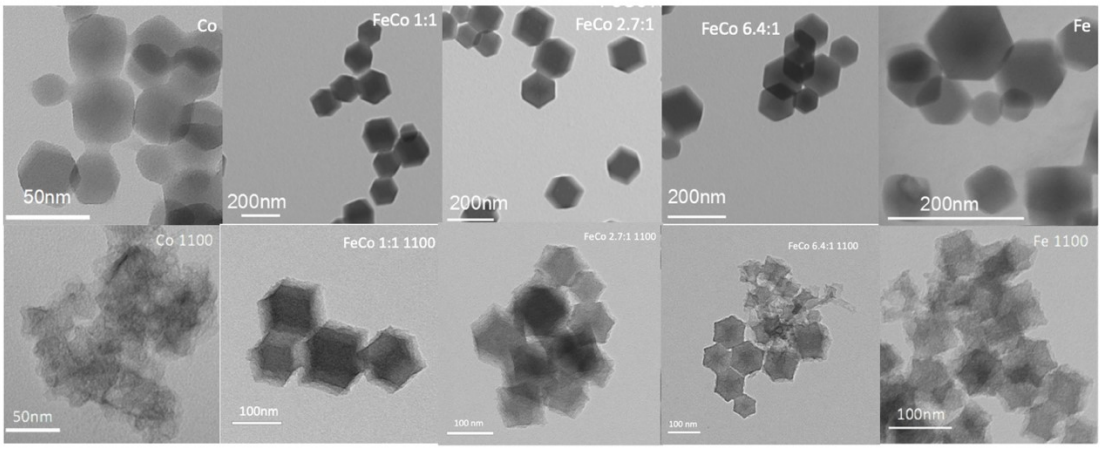

Figure 2-8 TEM images of Bimetal-ZIF nanocrystals before and after pyrolysis

The TEM images of single metal and bimetal ZIF nanocrystals before and after pyrolysis are showed in Figure 2-7 and Figure 2-8. Based on the Figure 2-7, before pyrolysis, only the Co-ZIF and the Fe-ZIF have the hexagonal shape while the Ni-ZIF, Cu-ZIF and Mn-ZIF don't have the hexagonal shape. After pyrolysis at 1100C, although the structures of Co-ZIF and the Fe-ZIF shrinked a little bit, they still show good cage-like structures. The cage-like structure may indicate the stability of the electrocatalyst so that they can have good electrocatalytic performance. Based

on the Figure 2-8, the hexagonal shapes of the Fe, Co-ZIF are even better than the single metal-ZIF. It indicates that the iron within the Fe, Co-ZIF has the ability to stabilize the structure before and after pyrolysis.

2.2.2. Inductively Coupled Plasma Mass Spectrometry (ICP-MS)

Table 2-3 ICP test result of single metal in the single metal-ZIF

Relative weight ratio	Co	Fe	Ni	Cu	Mn
	0.0135	0.0058	0.0037	0.0006	0.0008

Table 2-4 ICP test result of Fe, Co in the bimetal-ZIF

Fe/Co ratio	4:1	16:1	64:1
Actual Fe/Co ratio	1:1	2.7:1	6.4:1

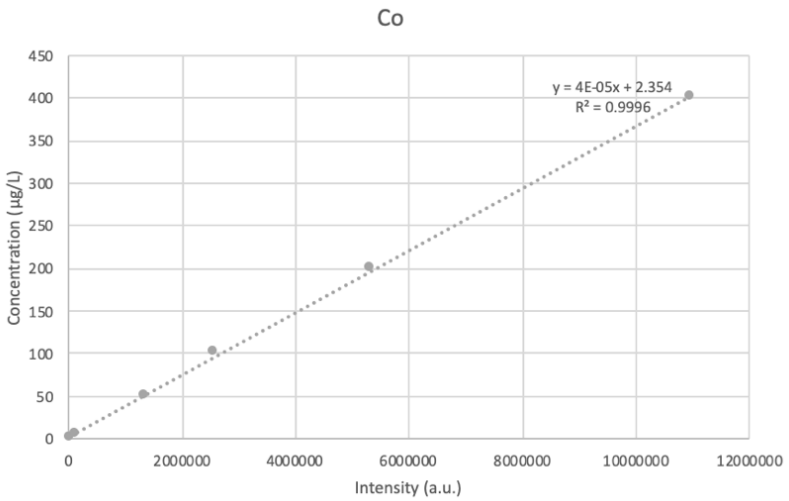

Figure 2-9 Calibration curves of Co concentration used in ICP test

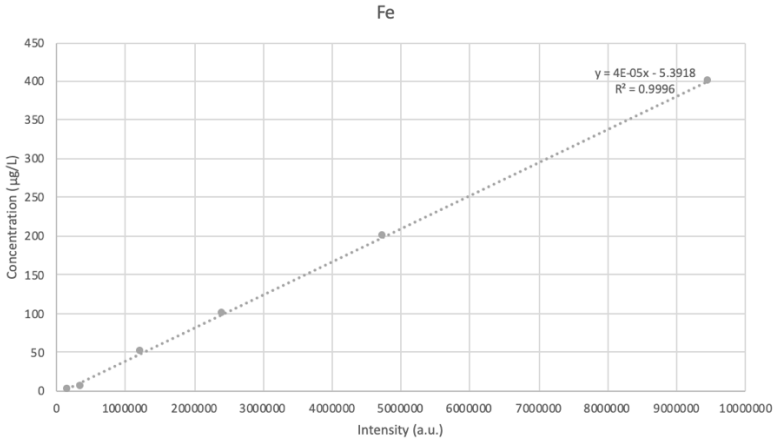

Figure 2-10 Calibration curves of Fe concentration used in ICP test

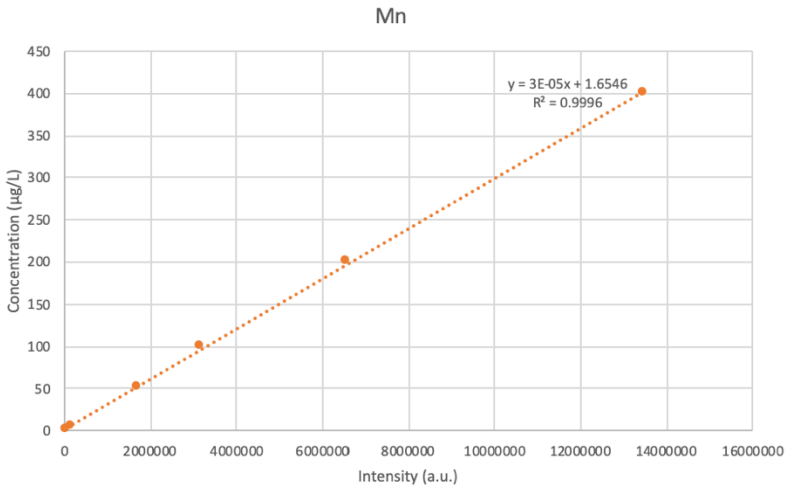

Figure 2-11 Calibration curves of Mn concentration used in ICP test

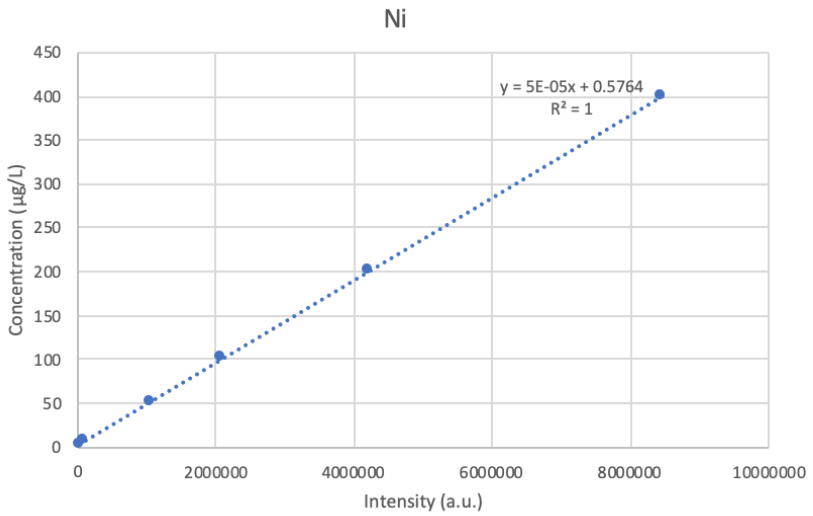

Figure 2-12 Calibration curves of Ni concentration used in ICP test

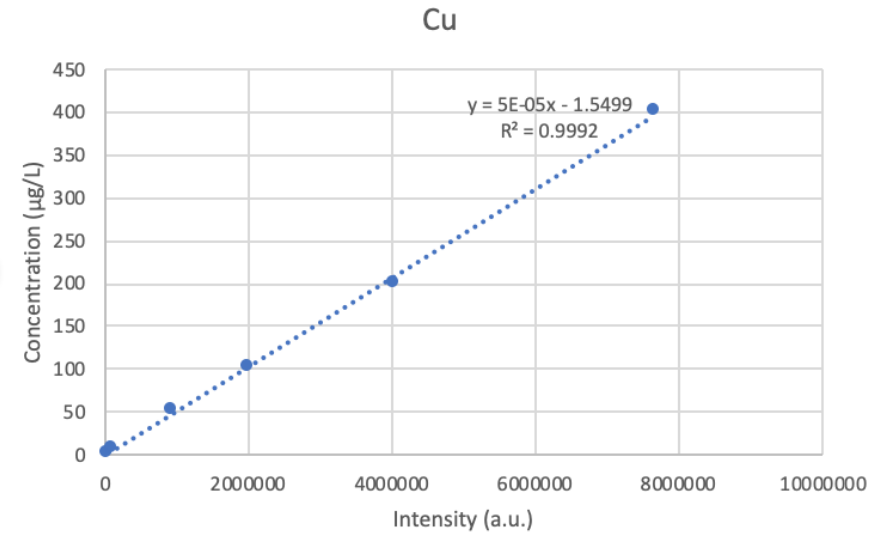

Figure 2-13 Calibration curves of Cu concentration used in ICP test

Based on the EDX results, we found out Co was much easier than other four metals to get into the ZIF-8 structure. In order to figure out how much metals get into the ZIf-8, the ICP-MS was operated. The ICP samples were immediately prepared after pyrolysis. The 2% hydrochloric acid was made as the base solution. 1ml of all commercial products (0.997ml for Mn) were added into 100ml volumetric flasks, then adding 2% hydrochloric acid to 100ml. Now we had the 10ul/ml solution of Fe, Co, Ni, Cu and Mn. The standard solution for Fe, Co, Ni, Cu and Mn were made by adding 0.05/ 0.5/ 1/ 2/ 4 ml above solution and dilute to 100ml in order to have the 5/ 50/ 100/ 200/ 400 ug/L. Around 1mg of all samples were weighted and acid wash by 0.5M sulfuric acid according to weight though centrifuging.

Table 2-3 shows the ICP test result of single metal in the single metal-ZIF. The cupper and manganese inside the ZIF-8 couldn't be like the cobalt one even the loadings of cupper salts and manganese salts increased. We varied the ratios of the Fe/Co from 4:1, 16:1 and 64:1 in order to let more Fe get access into the ZIF structure to stabilize the structure and enhance the catalytic performance. Table 2-4 shows the ICP test result of Fe, Co in the bimetal-ZIF that the actual Fe/Co ratio values for 4:1, 16:1 and 64:1 are 1:1, 2.7:1 and 6.4:1.

2.2.3. X-ray Powder Diffraction (XRD)

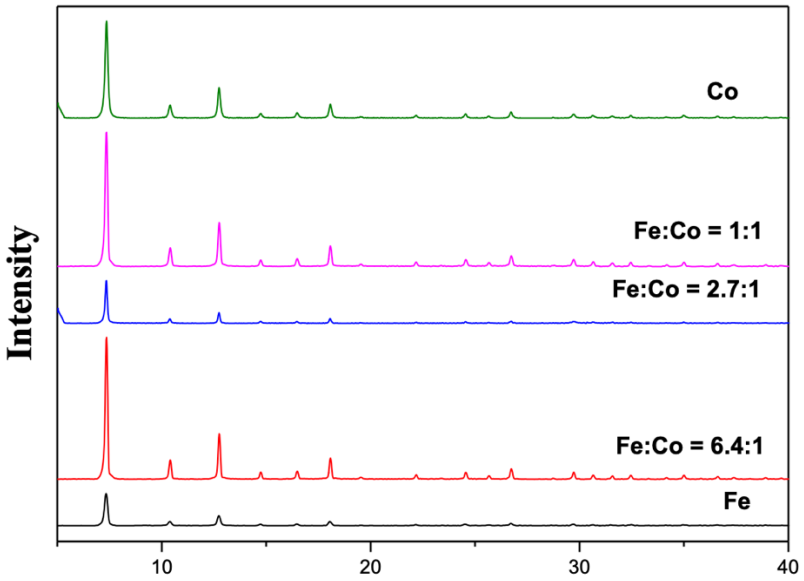

Figure 2-14 XRD of Bimetal-ZIF nanocrystals before pyrolysis

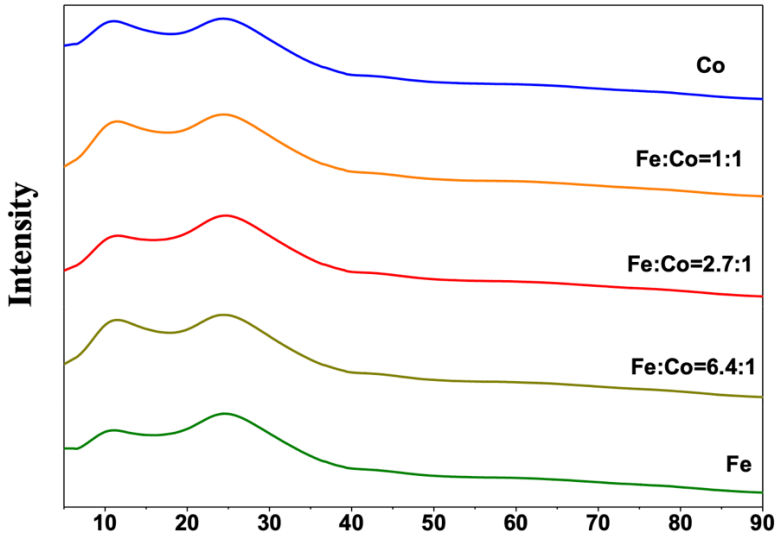

Figure 2-15 XRD of Bimetal-ZIF nanocrystals after pyrolysis

Figure 2-14 shows the XRD patterns for the Bimetal-ZIF nanocrystals before pyrolysis. The experimental XRD patterns of Co-ZIF, Fe, Co-ZIF with Fe/Co ratio from 1:1, 2.7:1, 6.4:1 and Fe-ZIF are shown from top to bottom respectively. Compare with the literature[24], it follows the ZIF structure XRD pattern. Figure 2-15 shows the XRD patterns for the Bimetal-ZIF nanocrystals after pyrolysis. Since the ZIF structure was collapsed and most part of the samples were carbon, there were no ZIF structure XRD pattern shown.

2.3. Electrochemical Measurements

A Metrohm PGSTAT302N potentiostat was used for the electrochemical studies. For the rotating disk electrode (RDE) measurements, a piece of glassy carbon (5 mm in diameter) was used as the working electrode, a Ag/AgCl redox couple as the reference electrode and a Pt wire as the counter electrode. The set up was shown in Figure 2-16.

For electrode preparation, the nanoparticles catalysts were dispersed in 10% iso-propanol (with 0.025 % Nafion) aqueous solutions at 1 mg/ml. The isopropanol was used to disper the nanoparticles while the nafion was used to let the nanoparticles attached on the surface of the working electrode. The mixtures were sonicated for about 20 minutes to allow formation of uniform ink. Typically, 80 ul of ink was dropped onto the surface of glassy carbon and was dried in air. The glassy carbon electrode with catalyst was shown in Figure 2-17. Cyclic voltammogram, ORR curve and Linear sweep voltammetry were recorded at 50 mV/s.

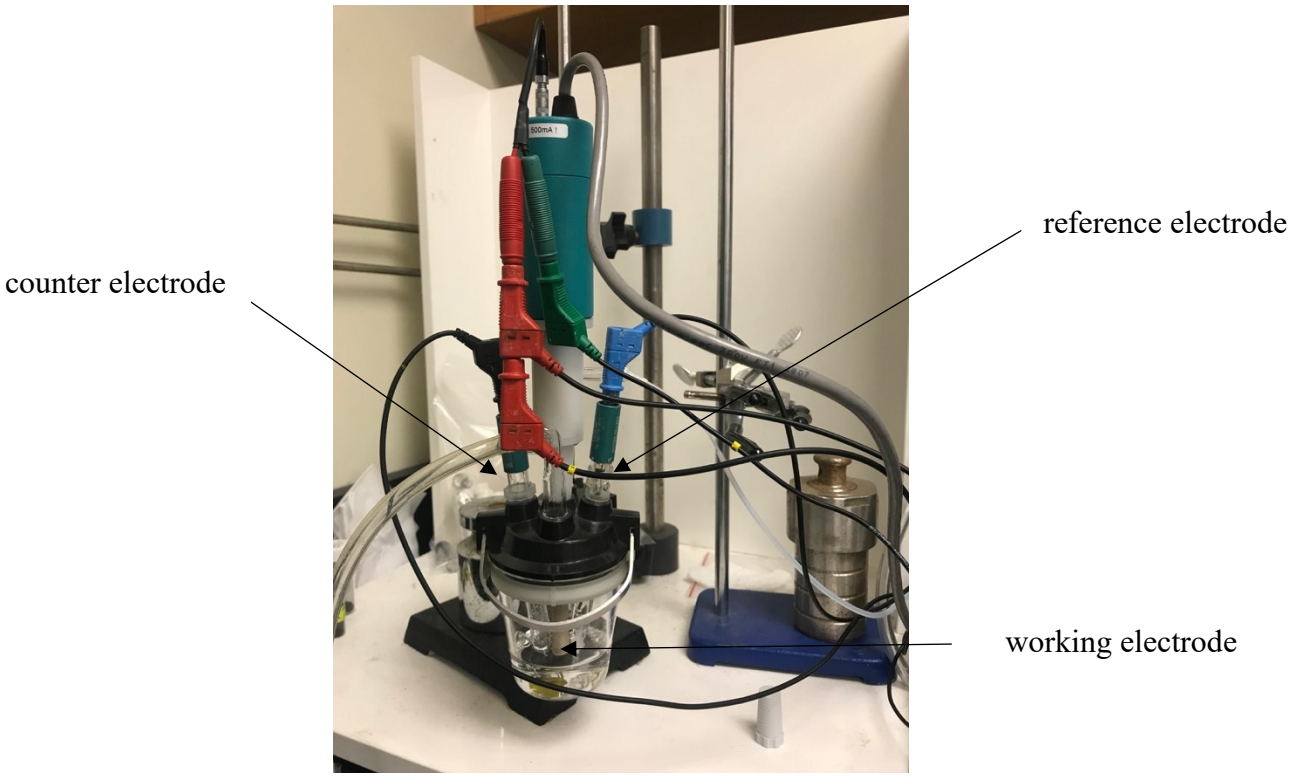

Figure 2-16. Set up for the electrochemical measurements

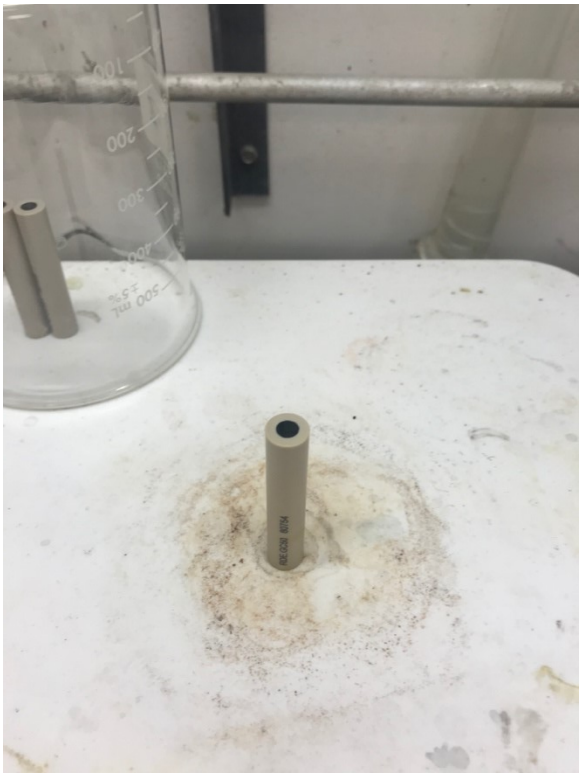

Figure 2-17. The glassy carbon electrode (working electrode) with catalyst

2.4. Temperature programmed desperation measurements

The AutoChem II 2920 is a highly automated catalyst characterization system. The operating procedures consist of three parts: prepare the samples, main TPD process and after the experiments.

2.4.1 Prepare the samples

The sample tube should be cleaned and adequately dried before use to obtain accurate analysis results. The interior of the sample tube was cleaned with the brush and it was rinsed thoroughly with DI water. Then it was rinsed again with isopropyl alcohol, using a waste container to collect used isopropyl alcohol. Dry, compressed nitrogen was used to dry the interior of the sample tube under a vent hood. After the sample tube was dry, 50 mg of sample would be loaded. A small amount of quartz wood was placed into the end of the clean, empty sample tube. The sample was well dispersed in the tube, not against the side or walls of the tube. Finally, the sample tube was assembled into the analyzer. It was shown in Figure 2-18

Figure 2-18 Sample tube assembly of temperature programmed desorption system

2.4.2 Main TPD process

After the samples tube was assembled into the analyzer. The main process of TPD was set up. For our experiments, the nitrogen TPD was used to replace oxygen TPD since the oxygen may cause damage to the TCD filament due to oxygen exposure while nitrogen is the one most similar to oxygen.

First, 7% of the hydrogen was flow to the sample at the rate of 30cm^3/min for 10 minutes. Then the temperature was raised to 600C at the ramping rate of 10C/min in order to get rid of the oxygen on the surface. Otherwise the oxygen will react with the carbon and finally turns to carbon

dioxide during the later temperature raising process. After that, the sample tube was saturated with helium at the rate of 5cm^3/min for 1 hour in order to get rid of the hydrogen on the surface.

After the sample pretreat, the temperature was cooled down to 35C. 5000 ppm nitrogen monoxide within the helium and nitrogen monoxide mixture gas (1% nitrogen monoxide and 99% helium) was flow to the sample surface for 30 minutes. The analysis valve changed from prepare mode to analyze mode and the blended carrier and loop gases went through the TCD.

Finally, the helium at the rate of 30cm^3/min was flow to the surface again for 1 hour to get rid of the excess nitrogen monoxide that didn't attached to the active sites of the catalysts. The temperature was raised to 550C with the ramping rate at 4C/min to process the NO TPD.

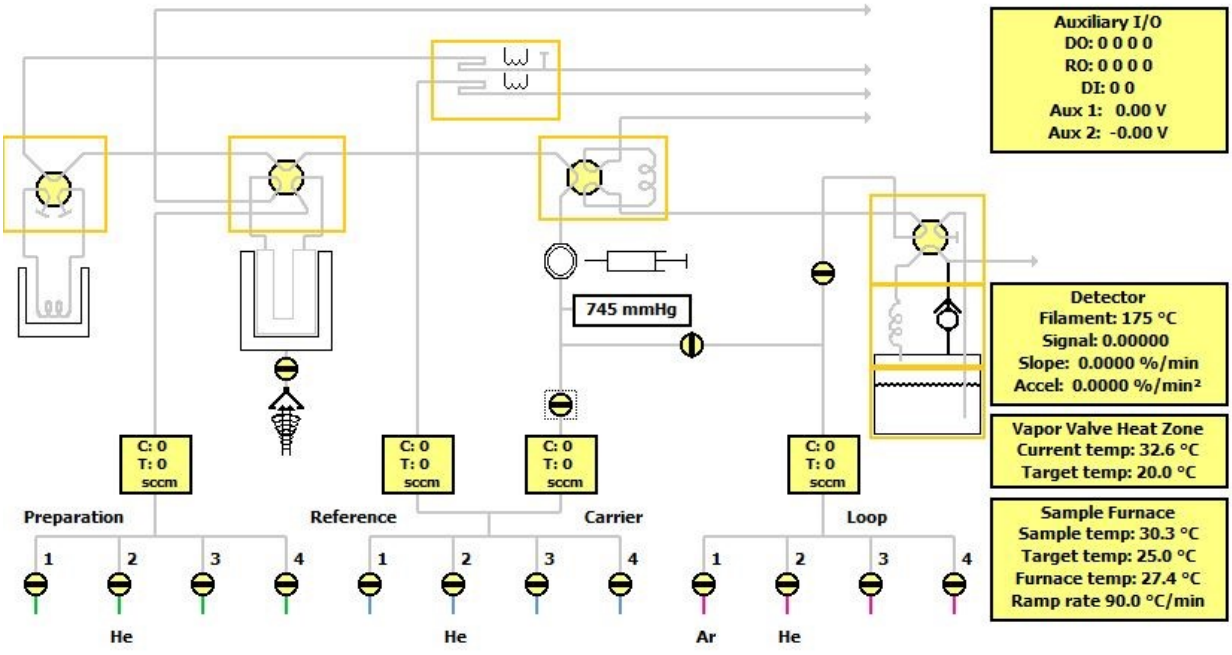

Figure 2-19 Command window of temperature programmed desorption

2.4.3 After the experiment

After the sample tube was cooled down, it should be cleaned after use to avoid contamination between each experiment. After the samples and quartz wood were removed from the sample tube, the sample tube should be rinsed with DI water and isopropyl alcohol respectively. Then the sample tube was placed in aqua regia overnight. After that, the empty sample tube needs to be heated in oven at 800C for 0.5 hr.

3 Discussion and results

3.1. Synthesis method

In order to find out the protocol to produce the catalyst with highest performance, we changed the temperature and protective gas during the pyrolysis process. Based on our experimental results, 1100C was the best pyrolysis temperature compare with 1000C and 900C. Also, nitrogen was the best protective gas compare with argon and ammonia. For the synthesis of Fe, Co-ZIF nanocrystal, we first tried to use the metal salts with nitrate ion. However, the precipitate was not formed. We switched the Fe $(NO_3)_2 \cdot 6H_2O$ to $Fe(acac)_3 \cdot 6H_2O$ to let the precipitate formed.

3.2. Electrochemical results analysis

The ORR catalytic activity of samples was investigated and compared with each other. In the cyclic voltammetry (CV) curves (figure 3-1), no obvious redox peak was detected for materials in Ar-saturated electrolyte. On the contrary, well-defined cathodic peaks occur when the electrolyte solution is saturated with O_2. The difference between them indicates comparable catalytic performance onsite potential.

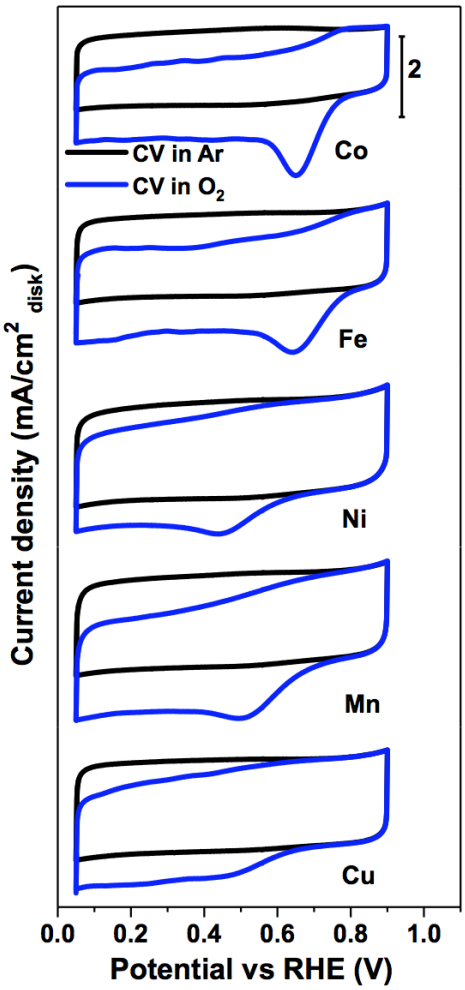

Figure 3-1 CV curves of Co/ Fe/ Ni/ Cu/ Mn-NC recorded in Argon- and O_2-saturated 0.1m H_2SO_4

Table 3-1 Cathodic peaks of single metal and nitrogen-doped NC-based electrocatalysts in O2-saturated (V)

	cathodic peaks in O2-saturated (V)
Co@N-C	0.65
Fe@N-C	0.63
Ni@N-C	0.44
Mn@N-C	0.50
Cu@N-C	0.42

Table 3-1 shows the cathodic peaks of 5 single metal and nitrogen-doped NC-based electrocatalysts in O_2-saturated. Based on these data, we could get the trend: Co > Fe > Mn > Ni > Cu which indicates that the Co- and Fe-NC are much better than the other three single metal NC. If we use the bulk metal as the catalyst, it should follow the order of Cu > Ni > Co > Fe > Mn. The difference between these two trends indicates the metal inside the M-N-C structure are not just metal particle but forming bonds with the nitrogen atoms.

Ring-disk electrode (RDE) experiments were carried out to confirm the catalytic activity of metal and nitrogen-doped carbon. The linear sweep voltammetry (LSV) curves shown in Figure 3-2 give us the onset and a half-wave potential. With the same onsite potential, the half-wave potential indicates the catalytic performance which follow the trend: Co > Fe > Mn > Ni > Cu[25].

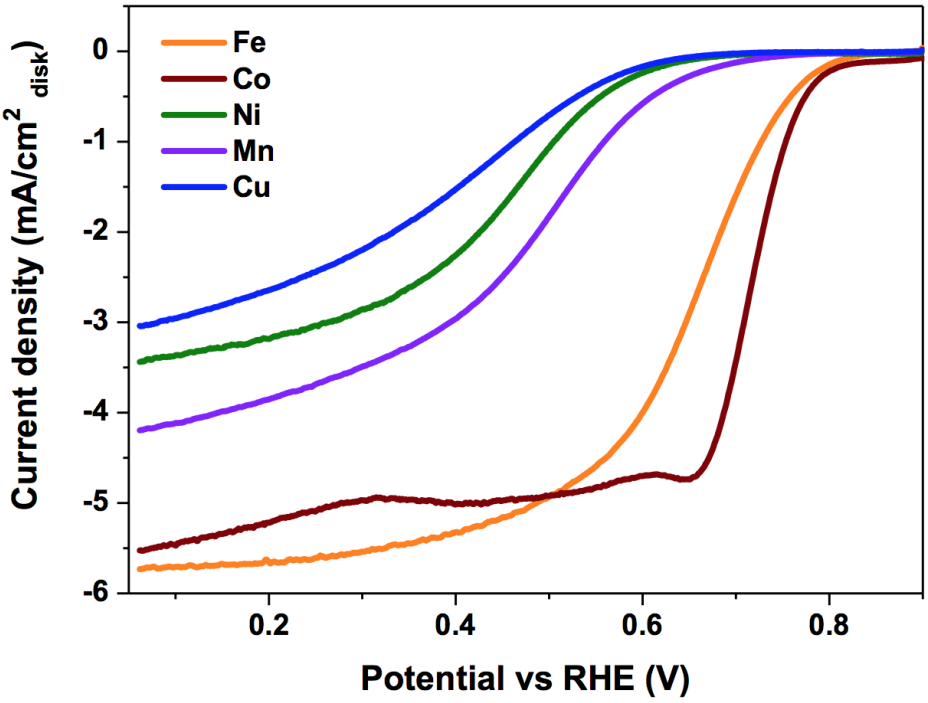

Figure 3-2 LSV curves for different materials in O_2- saturated 0.5M H_2SO_4 with rotation rate of 1600 rpm.

The LSV polarization curves of 5 single metal NC catalysts at different rotation rates, and the corresponding Koutecky–Levich (K–L) plots are shown in Figure 3-3 and Figure 3-4. With increasing rotation rate, no change is observed for the onset potential, while the current density increases because mass transport is improved at a higher rate. The Koutecky-Levich analysis is used to calculate the electron transfer number for ORR. There are two main products of ORR, water and hydrogen peroxide. If oxygen transform to water, it will be a 4 electrons process and for a hydrogen peroxide it will be a 2 electrons process. The 4 electrons process is more ideal than 2 electron process for ORR, so a higher electron transfer number indicate a higher catalysis activity.

We use the KL equation to calculate the electron transfer numbers for all samples. According to the data iron and cobalt has the highest number which means it has the highest catalytic activity.

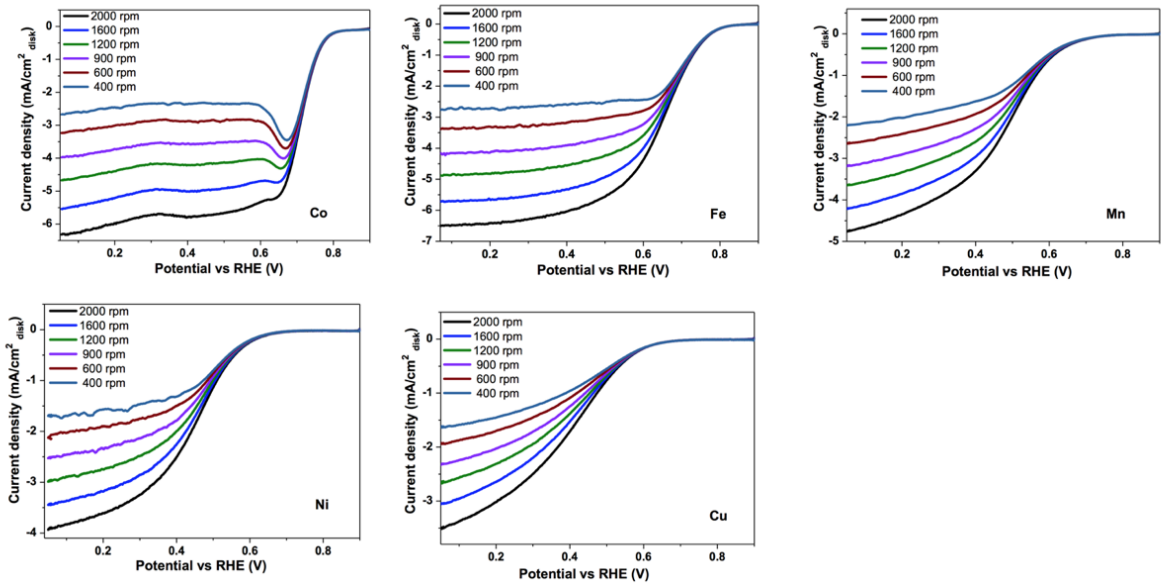

Figure 3-3 LSV curves of 5 single metal NC measured at different rotation rates

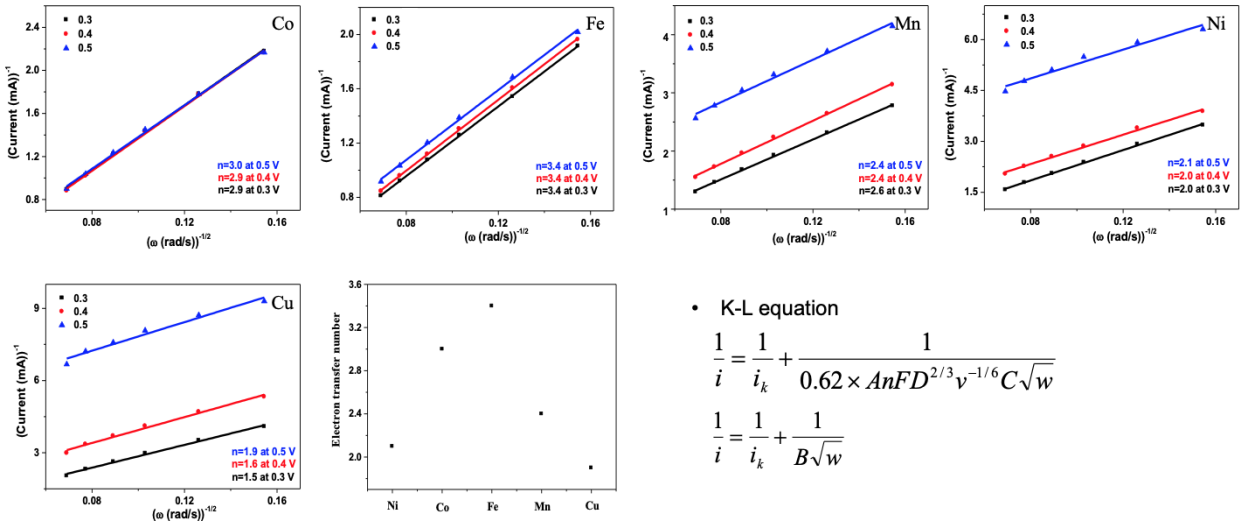

Figure 3-4 LSV curves of 5 single metal NC measured at different rotation rates and the volcano plot of electron transfer numbers for all samples

Based on the TEM, ICP-MS, CV, LSV and K-L analysis, the Co- and Fe-NC were proved to have greater performance than the Mn-/Ni-/Cu- NC. To improve the performance even further we tried to make the Co, Fe-NC bimetal catalysts with different ratio of Fe/Co. Figure 3-5 shows the CV curves, no OH adsorption peak or CO stripping peak was detected for materials in Ar-saturated and CO-saturated electrolyte. While for Pt/C electrocatalysts, the OH adsorption peak will appear at 0.8V and CO stripping peaks will appear at 0.85V. The difference indicates the electrocatalyst we made has a different mechanism compare with the Pt/C.

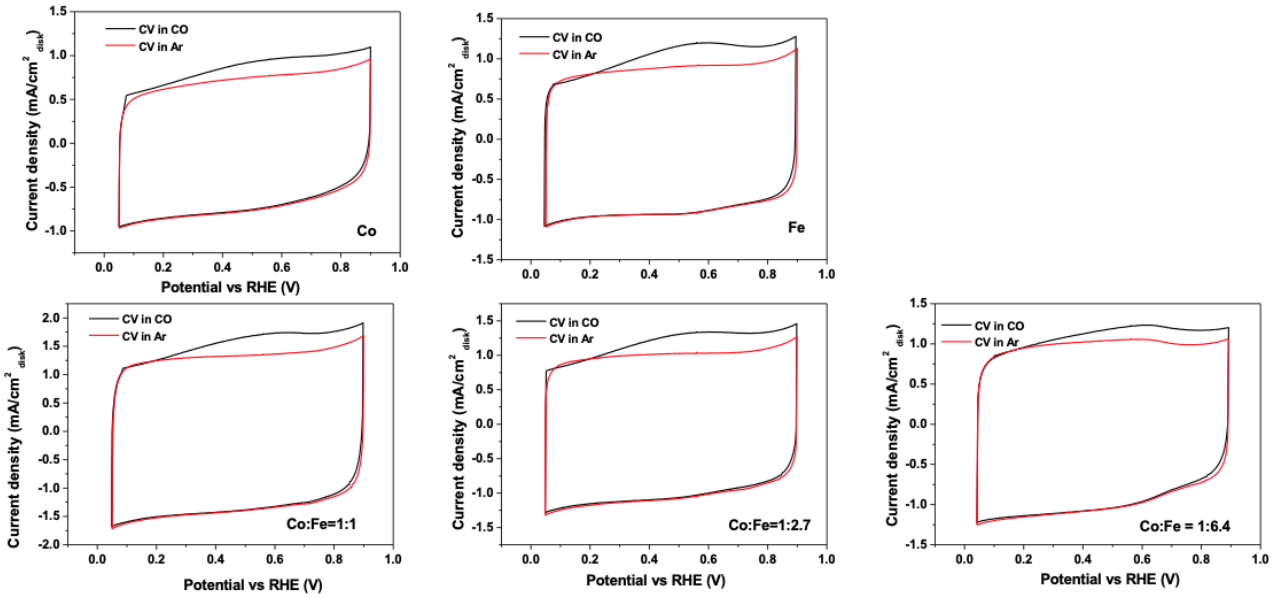

Figure 3-5 CV curves of Co/ Fe/ CoFe -NC recorded in Argon- and carbon monoxide -saturated 0.5M H_2SO_4

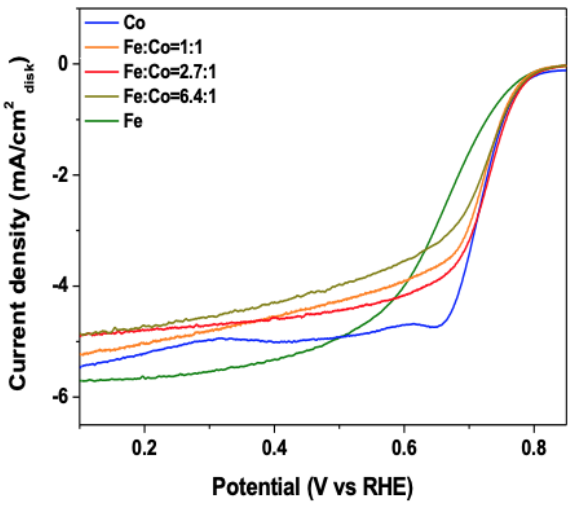

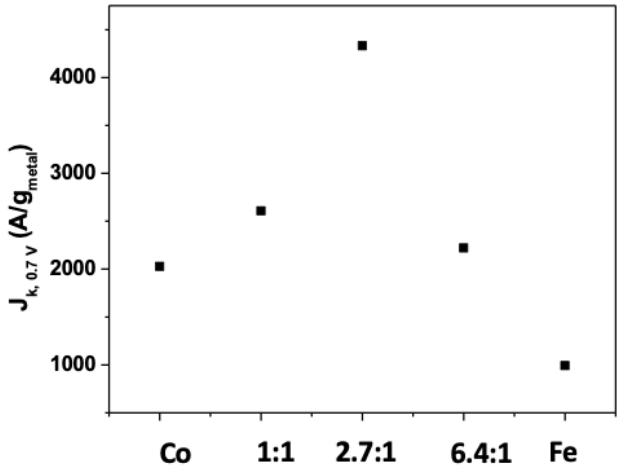

Figure 3-6 LSV curves for different materials in O_2- saturated 0.5M H_2SO_4 with rotation rate of 1600 rpm.

Figure 3-7 Volcano plot for the absolute current density at 0.7

Figure 3-6 and Figure 3-7 show the Fe, Co-NC with Fe/Co at 2.7:1 has the best catalytic performance based on the half wave potentials.

The LSV polarization curves of Co-/Fe-/Fe, Co- NC catalysts at different rotation rates, and the corresponding Koutecky–Levich (K–L) plots are shown in Figure 3-8 and Figure 3-9. With increasing rotation rate, no change is observed for the onset potential, while the current density increases because mass transport is improved at a higher rate. For the K-L analysis, the electron transfer number of Fe, Co-NC are between Fe-NC and Co-NC. Adding Iron component causes the electron number increases.

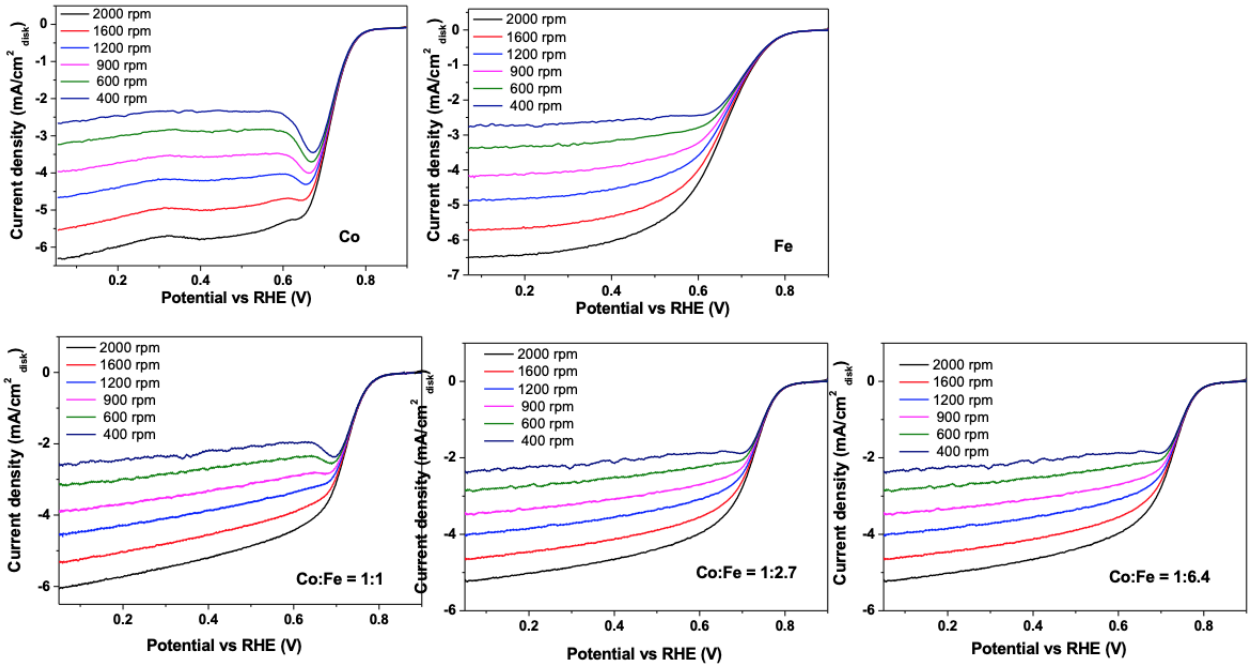

Figure 3-8 LSV curves of samples measured at different rotation rates

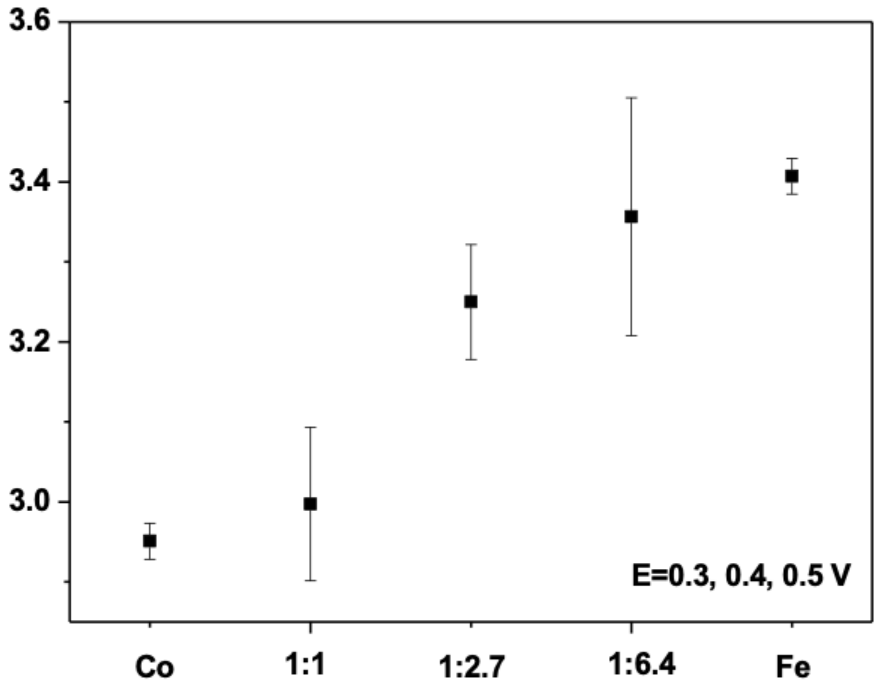

Figure 3-9 Electron transfer numbers for all samples

3.3. Temperature programmed desorption results analysis

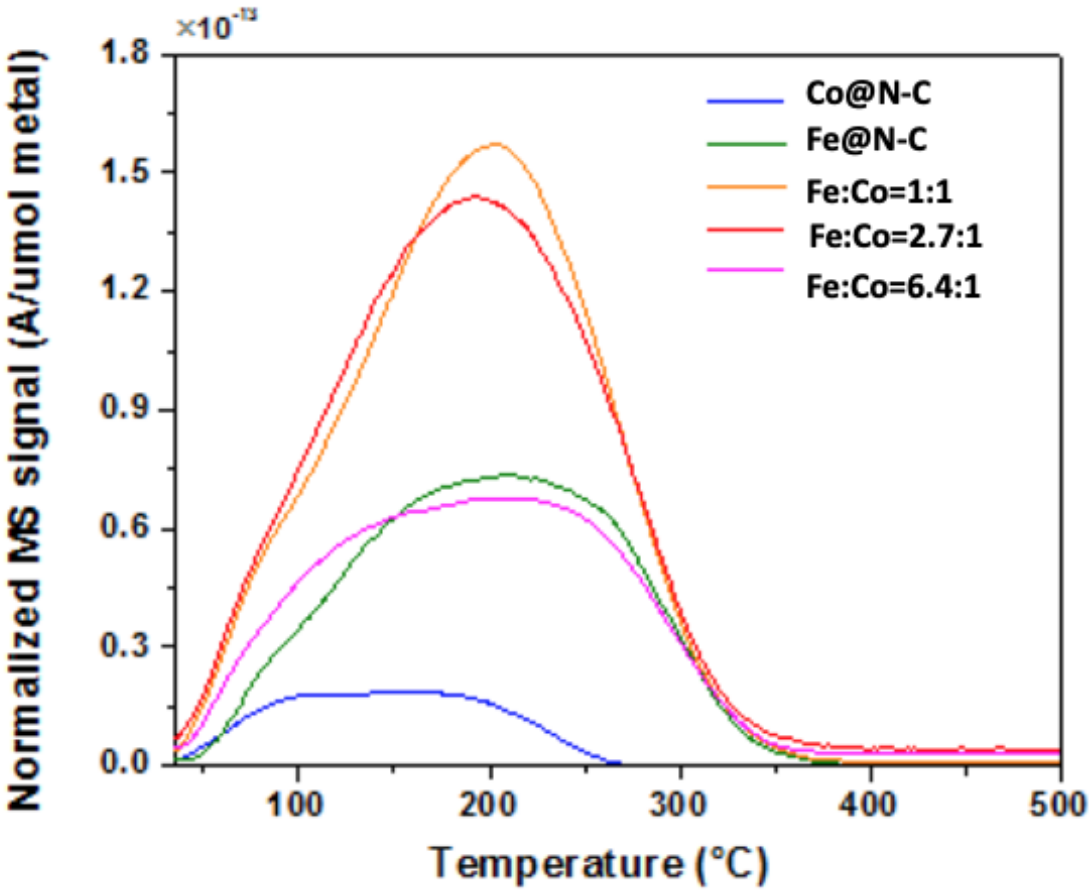

Figure 3-10 Temperature programmed desorption analysis for bimetal NC

The nitrogen monoxide TPD results show that the nitrogen monoxide was desorbed at 150 °C for Co@N-C and 220 °C for Fe@N-C while for the Fe, Co@N-C, the nitrogen monoxide was desorbed at 210 °C. The temperature difference between the single and bimetal nitrogen carbon indicates there are new active sites form for Fe, Co@N-C. Also, the area of the MS signal normalized by micromole metal shows that the number of active sites increase.

4. Conclusions

We successfully synthesized five single-metal and one bimetal –ZIF nanomaterials. The electrocatalysts were characterized by Transmission Electron Microscopy (TEM), Inductively Coupled Plasma Mass Spectrometry (ICP-MS) and X-ray Diffraction (XRD). ORR catalytic activities were investigated by cyclic voltammetry (CV) curves, linear sweep voltammetry (LSV) curves and Koutecký–Levich Analysis (K-L analysis). Active sites of the electrocatalysts were analyzed by TPD measurements.

5. References

1. "NIST: NIF - PEM Fuel Cells". Physics.Nist. Gov, 2019, https://physics.nist.gov/MajResFac/NIF/pemFuelCells.html.
2. Wang, Yun; Chen, Ken; Mishler, Jeffrey; Chan Cho, Sung; and Cordobes Adroher, Xavier, "A review of polymer electrolyte membrane fuel cells: Technology, applications, and needs on fundamental research" (2011). US Department of Energy Publications. 132. http://digitalcommons.unl.edu/usdoepub/132
3. Wu, Gang, and Piotr Zelenay. "Nanostructured Nonprecious Metal Catalysts For Oxygen Reduction Reaction". Accounts Of Chemical Research, vol 46, no. 8, 2013, pp. 1878-1889. American Chemical Society (ACS), doi:10.1021/ar400011z.
4. "Platinum's Fuel-Cell Car Bonanza Proves Elusive". U.S., 2019, https://www.reuters.com/article/us-platinum-fuelcells-analysis/platinums-fuel-cell-car-bonanza-proves-elusive-idUSKCN1GL1DG.
5. Gasteiger, Hubert A. et al. "Activity Benchmarks And Requirements For Pt, Pt-Alloy, And Non-Pt Oxygen Reduction Catalysts For Pemfcs". Applied Catalysis B: Environmental, vol 56, no. 1-2, 2005, pp. 9-35. Elsevier BV, doi:10.1016/j.apcatb.2004.06.021.

6. Gasteiger, Hubert A., and Nenad M Marković. "Just A Dream—Or Future Reality?". Science, vol 324, no. 5923, 2009, pp. 48-49. American Association For The Advancement Of Science (AAAS), doi:10.1126/science.1172083.

7. Zhang, Hanguang et al. "Engineering Nanostructures Of PGM-Free Oxygen-Reduction Catalysts Using Metal-Organic Frameworks". Nano Energy, vol 31, 2017, pp. 331-350. Elsevier BV, doi:10.1016/j.nanoen.2016.11.033.

8. Sahraie, Nastaran Ranjbar et al. "Quantifying The Density And Utilization Of Active Sites In Non-Precious Metal Oxygen Electroreduction Catalysts". Nature Communications, vol 6, no. 1, 2015. Springer Nature, doi:10.1038/ncomms9618.

9. Zhou, C. "Modulated Chemical Doping Of Individual Carbon Nanotubes". Science, vol 290, no. 5496, 2000, pp. 1552-1555. American Association For The Advancement Of Science (AAAS), doi:10.1126/science.290.5496.1552.

10. Lee, Sang Uck et al. "Designing Nanogadgetry For Nanoelectronic Devices With Nitrogen-Doped Capped Carbon Nanotubes". Small, vol 5, no. 15, 2009, pp. 1769-1775. Wiley, doi:10.1002/smll.200801938.

11. MATTER, P et al. "The Role Of Nanostructure In Nitrogen-Containing Carbon Catalysts For The Oxygen Reduction Reaction". Journal Of Catalysis, vol 239, no. 1, 2006, pp. 83-96. Elsevier BV, doi:10.1016/j.jcat.2006.01.022.

12. Wu, Gang et al. "Well-Dispersed High-Loading Pt Nanoparticles Supported By Shell−Core Nanostructured Carbon For Methanol Electrooxidation". Langmuir, vol 24, no. 7, 2008, pp. 3566-3575. American Chemical Society (ACS), doi:10.1021/la7029278.

13. Peng, Hongliang et al. "Effect Of Transition Metals On The Structure And Performance Of The Doped Carbon Catalysts Derived From Polyaniline And Melamine For ORR Application". ACS Catalysis, vol 4, no. 10, 2014, pp. 3797-3805. American Chemical Society (ACS), doi:10.1021/cs500744x

14. Zhang, Hui-Juan et al. "3D Non-Precious Metal-Based Electrocatalysts For The Oxygen Reduction Reaction In Acid Media". International Journal Of Hydrogen Energy, vol 35, no. 15, 2010, pp. 8295-8302. Elsevier BV, doi:10.1016/j.ijhydene.2009.12.015.

15. Wu, Gang et al. "Synthesis–Structure–Performance Correlation For Polyaniline–Me–C Non-Precious Metal Cathode Catalysts For Oxygen Reduction In Fuel Cells". Journal Of Materials Chemistry, vol 21, no. 30, 2011, p. 11392. Royal Society Of Chemistry (RSC), doi:10.1039/c0jm03613g.

16. Wu, G. et al. "High-Performance Electrocatalysts For Oxygen Reduction Derived From Polyaniline, Iron, And Cobalt". Science, vol 332, no. 6028, 2011, pp. 443-447. American Association For The Advancement Of Science (AAAS), doi:10.1126/science.1200832

17. Khalid, Mohd. et al. "Uniformly Self-Decorated Co3o4 Nanoparticles On N, S Co-Doped Carbon Layers Derived From A Camphor Sulfonic Acid And Metal–Organic Framework Hybrid As An Oxygen Evolution Electrocatalyst". Journal Of Materials Chemistry A, vol 6, no. 25, 2018, pp. 12106-12114. Royal Society Of Chemistry (RSC), doi:10.1039/c8ta02926a
18. You, Bo et al. "Bimetal–Organic Framework Self-Adjusted Synthesis Of Support-Free Nonprecious Electrocatalysts For Efficient Oxygen Reduction". ACS Catalysis, vol 5, no. 12, 2015, pp. 7068-7076. American Chemical Society (ACS), doi:10.1021/acscatal.5b02325
19. Armel, Vanessa et al. "Structural Descriptors Of Zeolitic–Imidazolate Frameworks Are Keys To The Activity Of Fe–N–C Catalysts". Journal Of The American Chemical Society, vol 139, no. 1, 2016, pp. 453-464. American Chemical Society (ACS), doi:10.1021/jacs.6b11248.
20. Park, K. S. et al. "Exceptional Chemical And Thermal Stability Of Zeolitic Imidazolate Frameworks". Proceedings Of The National Academy Of Sciences, vol 103, no. 27, 2006, pp. 10186-10191. Proceedings Of The National Academy Of Sciences, doi:10.1073/pnas.0602439103

21. Bux, Helge et al. "Zeolitic Imidazolate Framework Membrane With Molecular Sieving Properties By Microwave-Assisted Solvothermal Synthesis". Journal Of The American Chemical Society, vol 131, no. 44, 2009, pp. 16000-16001. American Chemical Society (ACS), doi:10.1021/ja907359t.

22. "Chemisorption | Particle Testing Authority". Particletesting.Com, 2019, https://www.particletesting.com/chemisorption/.

23. Saliba, Daniel et al. "Crystal Growth Of ZIF-8, ZIF-67, And Their Mixed-Metal Derivatives". Journal Of The American Chemical Society, vol 140, no. 5, 2018, pp. 1812-1823. American Chemical Society (ACS), doi:10.1021/jacs.7b11589.

24. Schejn, Aleksandra et al. "Controlling ZIF-8 Nano- And Microcrystal Formation And Reactivity Through Zinc Salt Variations". Crystengcomm, vol 16, no. 21, 2014, pp. 4493-4500. Royal Society Of Chemistry (RSC), doi:10.1039/c3ce42485e

25. Kepp, Kasper P. "A Quantitative Scale Of Oxophilicity And Thiophilicity". Inorganic Chemistry, vol 55, no. 18, 2016, pp. 9461-9470. American Chemical Society (ACS), doi:10.1021/acs.inorgchem.6b01702.

Curriculum Vita

Pingfan Hu was born in Shanghai, China in 1994. He attended University of Illinois at Urbana-Champaign beginning in the fall of 2013 and graduated in the summer of 2017 major in chemical engineering and minor in geology. At University of Illinois at Urbana-Champaign, he worked on the project of design a plug-and-play pathway refactoring workflow based on Golden Gate reaction. Following completion of his undergraduate degree, Pingfan began his master program at Johns Hopkins University major in chemical engineering. In May of 2019 he became a master student of Dr. Chao Wang, studying nitrogen-coordinated metal electrocatalysts for oxygen reduction reaction.